SINTEF
PROCEEDINGS
2

Proceedings of the 12th International Conference on Computational Fluid Dynamics in the Oil & Gas, Metallurgical and Process Industries

Progress in Applied CFD – CFD2017

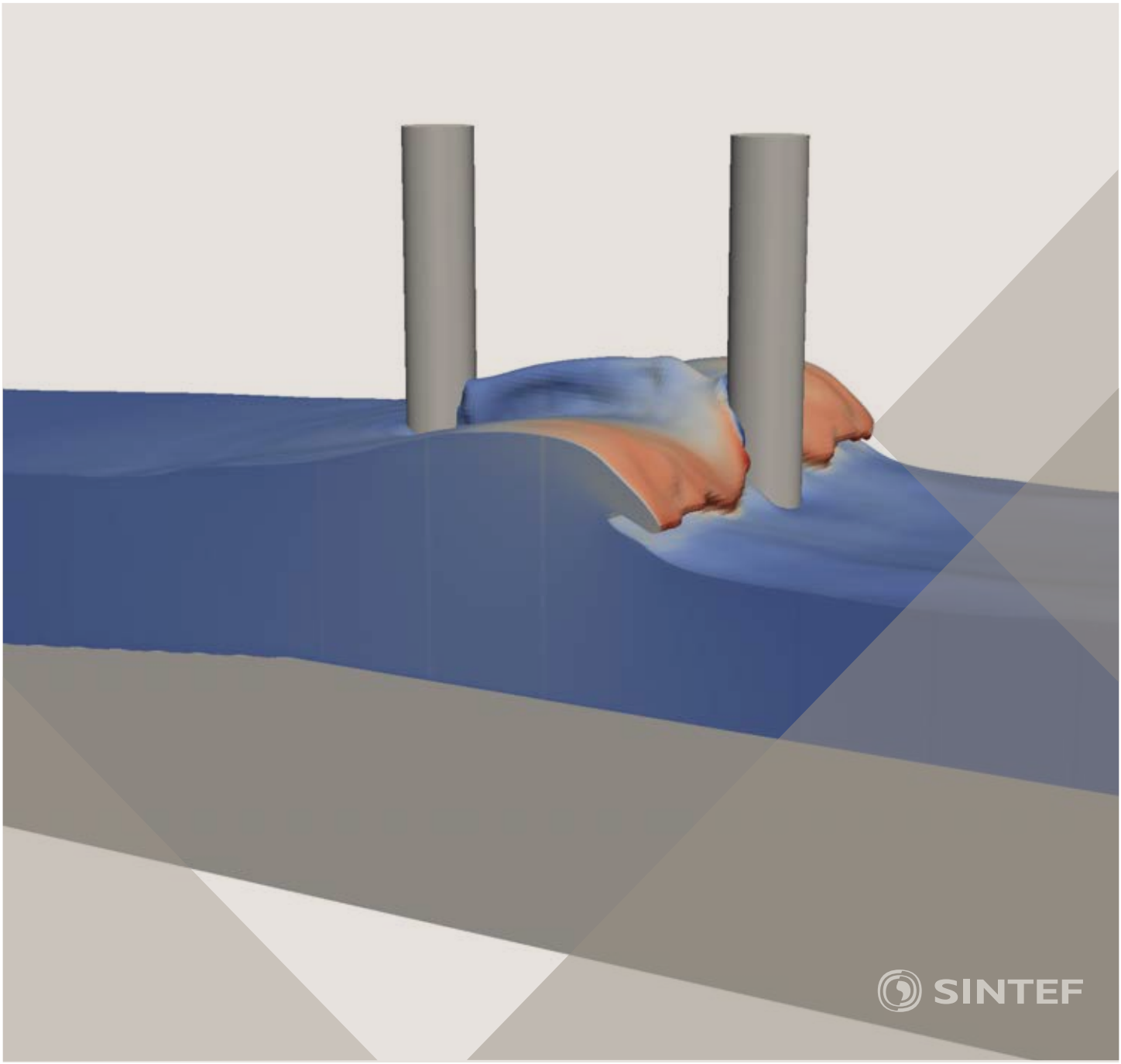

SINTEF Proceedings

Editors:
Jan Erik Olsen and Stein Tore Johansen

Progress in Applied CFD – CFD2017

Proceedings of the 12th International Conference on Computational Fluid Dynamics in the Oil & Gas, Metallurgical and Process Industries

SINTEF Academic Press

SINTEF Proceedings no 2
Editors: Jan Erik Olsen and Stein Tore Johansen
Progress in Applied CFD – CFD2017
Selected papers from 10th International Conference on Computational Fluid Dynamics in the Oil & Gas, Metallurgical and Process Industries

Key words:
CFD, Flow, Modelling

Cover, illustration: Arun Kamath

ISSN 2387-4295 (online)
ISBN 978-82-536-1544-8 (pdf)

SINTEF Academic Press
Address: Forskningsveien 3 B
PO Box 124 Blindern
N-0314 OSLO
Tel: +47 73 59 30 00
Fax: +47 22 96 55 08

www.sintef.no/byggforsk
www.sintefbok.no

SINTEF Proceedings
SINTEF Proceedings is a serial publication for peer-reviewed conference proceedings on a variety of scientific topics.
The processes of peer-reviewing of papers published in SINTEF Proceedings are administered by the conference organizers and proceedings editors. Detailed procedures will vary according to custom and practice in each scientific community.

PREFACE

This book contains all manuscripts approved by the reviewers and the organizing committee of the 12th International Conference on Computational Fluid Dynamics in the Oil & Gas, Metallurgical and Process Industries. The conference was hosted by SINTEF in Trondheim in May/June 2017 and is also known as CFD2017 for short. The conference series was initiated by CSIRO and Phil Schwarz in 1997. So far the conference has been alternating between CSIRO in Melbourne and SINTEF in Trondheim. The conferences focuses on the application of CFD in the oil and gas industries, metal production, mineral processing, power generation, chemicals and other process industries. In addition pragmatic modelling concepts and bio-mechanical applications have become an important part of the conference. The papers in this book demonstrate the current progress in applied CFD.

The conference papers undergo a review process involving two experts. Only papers accepted by the reviewers are included in the proceedings. 108 contributions were presented at the conference together with six keynote presentations. A majority of these contributions are presented by their manuscript in this collection (a few were granted to present without an accompanying manuscript).

The organizing committee would like to thank everyone who has helped with review of manuscripts, all those who helped to promote the conference and all authors who have submitted scientific contributions. We are also grateful for the support from the conference sponsors: ANSYS, SFI Metal Production and NanoSim.

Stein Tore Johansen & Jan Erik Olsen

Organizing committee:

Conference chairman: Prof. Stein Tore Johansen
Conference coordinator: Dr. Jan Erik Olsen
Dr. Bernhard Müller
Dr.Sigrid Karstad Dahl
Dr.Shahriar Amini
Dr.Ernst Meese
Dr.Josip Zoric
Dr.Jannike Solsvik
Dr.Peter Witt

Scientific committee:

Stein Tore Johansen, SINTEF/NTNU
Bernhard Müller, NTNU
Phil Schwarz, CSIRO
Akio Tomiyama, Kobe University
Hans Kuipers, Eindhoven University of Technology
Jinghai Li, Chinese Academy of Science
Markus Braun, Ansys
Simon Lo, CD-adapco
Patrick Segers, Universiteit Gent
Jiyuan Tu, RMIT
Jos Derksen, University of Aberdeen
Dmitry Eskin, Schlumberger-Doll Research
Pär Jönsson, KTH
Stefan Pirker, Johannes Kepler University
Josip Zoric, SINTEF

CONTENTS

DIRECT NUMERICAL SIMULATION OF THE EFFECTIVE DRAG IN GAS-LIQUID-SOLID SYSTEMS

Maike W. BALTUSSEN[1*], **J. A.M. KUIPERS**[1†], **Niels G. DEEN**[2‡]

[1]Multiphase Reactors Group, Eindhoven University of Technology, Postbus 513, 5600 MB Eindhoven, THE NETHERLANDS

[2]Multiphase and Reactive Flows Group, Eindhoven University of Technology, Postbus 513, 5600 MB Eindhoven, THE NETHERLANDS

[*] E-mail: m.w.baltussen@tue.nl
[†] E-mail: j.a.m.kuipers@tue.nl
[‡] E-mail: n.g.deen@tue.nl

ABSTRACT

Due to the increase in the oil prices and the depletion of the oil reserves, Fischer-Tropsch processes for the production of synthetic fuels, methanol synthesis and other gas-to-liquid processes are rapidly gaining interest. These reactions are commonly performed in slurry bubble columns, i.e. three-phase gas-liquid-solid reactors. Although slurry bubble columns are already widely used, challenging scale-up and operational issues are encountered when these reactors are used for the Fisher-Tropsch process. To improve the fundamental understanding of these complex reactors, this work focuses on the effective drag acting on particles and bubbles in dense flows, using Direct Numerical Simulations. We combined the Front Tracking method of Roghair *et al.* (2013b) and the second order implicit Immersed Boundary method of Deen *et al.* (2012), resulting in a resulting hybrid Front Tracking Immersed Boundary method that is able to simulate dense three phase flows and quantify the effects. For a system consisting of 2 mm bubbles and 1 mm particles, effective drag closures are developed for both the bubbles and the particles at several phase volume fractions. In future research, the developed methodology will be applied to study the effect of the bubble and particle size and their ratio as well as heat and mass transfer.

Keywords: Multiphase flow, Slurry bubble column, multiscale modeling, gas-liquid-solid flows, fluid structure interaction, Front Tracking, Immersed Boundary method .

NOMENCLATURE

Greek Symbols

α	Void fraction.
μ	Viscosity, $[\mathrm{Pa}\cdot\mathrm{s}]$.
ρ	Density, $[\mathrm{kg/m^3}]$.
σ	Surface tension coefficient, $[\mathrm{N/m}]$.
$\boldsymbol{\tau}$	Stress tensor, [Pa].
ϕ	Solid volume fraction.
ψ	Velocity component, $[\mathrm{m/s}]$.
ω	Rotational velocity, $[1/\mathrm{s}]$.

Latin Symbols

a, b, C	Coefficient.
d	Diameter, [m].
DNS	Direct Numerical Simulation.
Eo	Eötvös number, $g_z d_b^2 \Delta\rho/\sigma$.
$\mathbf{F}$	Force density or Force, $[\mathrm{N/m^3}]$ or [N].
FT	Front Tracking.
$\mathbf{g}$	Gravity acceleration, $[\mathrm{m/s^2}]$.
IB	Immersed Boundary.
I	Moment of inertia , $[\mathrm{kg}\cdot\mathrm{m^2}]$.
MCFD	Multiphase Computational Fluid Dynamics.
Mo	Morton number, $g_z \mu_l^4 \Delta\rho / \left(\rho_l^2 \sigma^3\right)$.
$\mathbf{n}$	Normal.
p	Pressure, [Pa].
t	Time, [s].
$\mathbf{r}$	Distance, [m].
Re	Reynolds number, $\rho\lvert\mathbf{v}\rvert d_b/\mu_l$.
$\mathbf{u}$	Liquid, fluid velocity , $[\mathrm{m/s}]$.
$\mathbf{v}$	Bubble velocity, $[\mathrm{m/s}]$.
V	Volume, $[\mathrm{m^3}]$.
$\mathbf{w}$	Particle velocity, $[\mathrm{m/s}]$.

Sub/superscripts

b	Bubble.
B	Buoyancy.
c	Central.
col	Due to particle-particle collisions.
D	Drag.
g	Gas phase.
l	Liquid phase.
nb	Neighboring.
P	Pressure.
rel	Relative.
s	Solid phase.
z	Direction of the gravitation.
σ	Surface tension.
∞	Single bubble or particle infinite liquid.

INTRODUCTION

The interest in Fischer-Tropsch processes for the production of synthetic fuels, methanol synthesis and other prominent gas-to-liquid processes has rapidly expanded in recent years, due to depletion of oil reserves and increasing oil prices. In these gas-to-liquid processes, a reactant gas is converted into liquid products over a solid catalyst. These type of three-phase gas-liquid-solid processes are often performed in slurry bubble columns. To accurately scale-up and design these columns, the fundamental understanding of the complex three phase interactions needs to be improved (Kantarci *et al.*, 2005; Wang *et al.*, 2007; Yang *et al.*, 2007; Pan *et al.*, 2016).

The introduction of particles in a bubble column causes a decrease in the bubble size and and increase in the void fraction. Besides, the bubble rise velocity decreases with increasing solids volume fraction even when neutrally buoyant particles are used (Kantarci *et al.*, 2005; Wang *et al.*, 2007; Hooshyar *et al.*, 2013; Baltussen *et al.*, 2013; Pan *et al.*, 2016). By using neutrally buoyant particles, Hooshyar *et al.* (2013) reported that the interaction mechanism depends on the Stokes relaxation time of the particles. When the Stokes relaxation time is relatively small, the bubble rise velocity is only affected via an increase in the apparent viscosity. For larger particles, which also have a larger Stokes relaxation time, the bubble rise velocity is only slightly influenced by the change in the apparent viscosity, while the main effect is caused by the encounters between the particles and the bubbles.

Because slurry bubble columns are often several meters in diameter and tens of meters in height, it is not possible to resolve all the details of the bubble-particle interactions for a full slurry bubble column. Therefore, a multiscale modeling approach is used to simulate industrial size columns. In this approach, coarse grained models, which do not capture the the particle/bubble scale transport phenomena (like the Euler-Lagrange or Euler-Euler models), need closures for the bubble-bubble, bubble-particle and particle-particle interactions. This effective drag acting on the particles and the bubbles in dense can will be determined using smaller scale models, like the novel hybrid Direct Numerical Simulation (DNS) approach in this work (van Sint Annaland *et al.*, 2003; Deen *et al.*, 2004; Yang *et al.*, 2007; Raessi *et al.*, 2010; Roghair *et al.*, 2011; Baltussen *et al.*, 2013; Pan *et al.*, 2016).

Several hybrid three-phase DNS methods have already been developed. Li *et al.* (2001) combined a Euler-Lagrange model for the particles with a DNS method for the bubbles. Although the particles are in reality much smaller than the bubbles, the method still requires closures for the solid-liquid interactions. Ge and Fan (2006), Jain *et al.* (2012) and Baltussen *et al.* (2016) combined a front capturing technique (Level-Set, Volume of Fluid and Volume of Fluid methods, respectively) for the gas-liquid interfaces with an Immersed Boundary (IB) method, to enforce the no-slip boundary condition at the surface of rigid immersed bodies. The disadvantage of these front capturing methods is the numerical coalescence which occurs when bubbles are close to each other. To overcome the numerical coalescence, Deen *et al.* (2009) and Baltussen *et al.* (2013) combined the Front Tracking (FT) method with a IB method. In FT, the bubbles are tracked directly using a triangular mesh. However, the separate mesh for each of the bubbles, the used FT currently prevents all coalescence between bubbles.

In this work, the swarm effects on the apparent drag of the bubbles and the particles is studied, requiring a constant bubble size during the simulation to facilitate the ease of interpretation. Therefore, we combined the FT method of Roghair *et al.* (2013a) with the second order implicit IB method of Deen *et al.* (2012). This specific IB method is chosen, because the method does not require a calibration of the effective particle size.

This paper starts with a short discussion of the applied numerical method and a short overview of the chosen numerical parameters. Subsequently, the effect of the void fraction and the solids volume fraction on the effective drag of the bubbles and the particles is discussed.

NUMERICAL METHOD

Our novel hybrid three phase DNS method is a combination of the FT method of Roghair *et al.* (2013a) and the second order IB method of Deen *et al.* (2012). Here, we present only a brief discussion of both methods, particularly focusing on the combination of both methods and the modification required to enable the calculation of three-phase systems.

The hybrid FT-IB model solves the continuity equation, equation 1, and the Navier-Stokes equations, equation 2, assuming incompressible flow:

$$\nabla \cdot \mathbf{u} = 0 \tag{1}$$

$$\rho \frac{\partial \mathbf{u}}{\partial t} = -\nabla p - \rho \nabla \cdot (\mathbf{u}\mathbf{u}) - \nabla \cdot \boldsymbol{\tau} + \rho \mathbf{g} + \mathbf{F}_\sigma \tag{2}$$

Because the velocity field is continuous across the gas-liquid interface, the Navier-Stokes equations can be solved using an one-field approximation. The surface tension at the gas-liquid interface is taken into account by an extra force density, $\mathbf{F}_\sigma$, which is introduced near the interface. This force is directly calculated from the triangular mesh by summing the tensile forces exerted by the three neighboring markers, triangular element, on a reference marker and subsequent force mapping to the Eulerian grid using mass-weighing (Dijkhuizen *et al.*, 2010b; Roghair, 2012). To alleviate the parasitic currents that arise due to the mismatch between the discretisation of the surface tension and the pressure field, the surface tension calculations is augmented with the so-called "pressure-jump correction" (Renardy and Renardy, 2002; Francois *et al.*, 2006; Dijkhuizen *et al.*, 2010b). The local density and viscosity are obtained by normal and harmonic averaging, respectively.

The no-slip boundary condition at the particle surface is taken into account implicitly. At the level of the discretised Navier-Stokes equations, each velocity component at a certain node in the fluid, ψ_c, can be described as a function of the velocity components of the neighboring nodes, ψ_{nb}, with equation 3.

$$a_c \psi_c + \sum_{nb} a_{nb} \psi_{nb} = b_c \tag{3}$$

where the coefficients a_{nb} indicate the coupling of the velocity at node c with the velocities of the neighboring nodes, nb.

Using a second order (1D) polynomial fit, each neighboring fluid node inside a particle can be eliminated from equation 3. Together with the local velocity field and the velocity at the particle surface, the coefficients of the two velocity nodes involved in the polynomial fit are adjusted. A similar function is obtained for fluid nodes that are in close proximity of two particles, when there is only 1 grid point in between the particles, by using the velocity of the central node and the velocity of both particles. Because both equations are singular when the particle surface is close to the central cell, a linear fit is used when the distance between the surface and the central point is less than 10^{-4} times the grid size.

The velocity field given by equation 2 is obtained on a staggered grid using a projection-correction method. In the projection step, all terms in this equation are treated explicitly except for the diffusion term, which is treated semi-implicitly. The implicit part of the diffusion term is chosen such that it only depends on the velocity component that is solved for, whereas the remaining (small) terms are treated explicitly. The diffusion terms are discretised using

a second order central difference scheme, while a second order flux-delimited Barton scheme is used for the convective terms. The projected velocity field is corrected to satisfy the continuity equation (equation 1). The equations in both the projection step and the correction step are solved using a OpenMP parallelised block ICCG matrix solver.

Particles

When the velocity field is calculated, the positions of the particles, m, are updated by solving the Newtonian equations of motion:

$$V_m \rho_m \frac{d\mathbf{w}_m}{dt} = m\mathbf{g} + \oint_{\Gamma_m} -(\boldsymbol{\tau}\cdot\mathbf{n})dS + \iiint_{\Omega_m} -\nabla p dV + F_{d,col} \tag{4}$$

$$I_m \frac{d\boldsymbol{\omega}_m}{dt} = \oint_{\Gamma_m} (\mathbf{r}_{i,j,k} - \mathbf{r}_m) \times -(\boldsymbol{\tau}\cdot\mathbf{n})dS \tag{5}$$

where the moment of inertia is given by:

$$I_m = \frac{1}{10} V_m \rho_m d_m^2 \tag{6}$$

In the three-phase system, the transpose part of the Stokes stress tensor in equation 4 and 5 should be included, because the viscosity is not constant. Both the pressure gradient and the velocity gradients, which are needed in the stress tensor, can be obtained directly from the second order fit, which was used to apply the no-slip boundary condition.

In the continuous limit, the calculation of the pressure force can be performed with either a surface integral or a volume integral using Gauss's theorem. Although the pressure inside the particle is unknown, the volume integral of the pressure gradient over the total particles will effectively result in a calculation depending on the pressures outside the particle due to the employed discretisation. When the calculation via the surface integral and the volume integral are compared with the results of Zick and Homsy (1982), the calculation of the force via the surface integral is not able to accurately capture the drag of a particle in a dense array. Therefore, the drag force will be calculated via the volume integral in this paper.

The interactions between the particles are included using a hard sphere model (Hoomans *et al.*, 1996). Therefore the drag force as discussed before does not include the collisions with other particles. However, the collisions with the bubbles are not separately treated and therefore their effects will be lumped in the drag force.

Bubbles

Following the update of the particle positions and velocities, the position of the bubbles is updated. Every marker point at the surface is displaced separately with the local velocity, which is interpolated from the Eulerian grid using cubic spline interpolation, by fourth order Runga-Kutta time stepping. Because each marker point is advected separately, the bubbles will change both its position and its shape. Nevertheless, this also changes the distance between the marker points leading to a decreased surface mesh quality. To restore the mesh quality, the surface is remeshed, using four elementary operations: edge splitting, edge collapsing, edge swapping and smoothing (Roghair, 2012).

Due to the separate advection of the marker points and the remeshing, small volume changes in the bubble volume arise, which accumulate over the total simulation time. To locally restore the volume losses during the remeshing a smoothing procedure described by Kuprat *et al.* (2001) is implemented. Moreover, the volume changes due to the separate advection of each marker are compensated by distributing the lost volume over all the interface cells. This procedure might cause unphysical overlap with other bubbles and particles. Marker points that are close to another bubble or particle, within the maximal edge length of a marker, are therefore excluded from this operation.

Table 1: Simulation settings for the base case of the slurry bubble swarms.

Property	Value	Unit
Void fraction, α	0.30	
Solid volume fraction, ϕ	0.05	
Computational grid	171	
Grid size	$1.0\cdot10^{-4}$	m
Time step	$1.0\cdot10^{-5}$	s
Bubble diameter	$2.0\cdot10^{-3}$	m
Particle diameter	$1.0\cdot10^{-3}$	m
Liquid density	$1.0\cdot10^{3}$	kg/m^3
Liquid viscosity	$1.0\cdot10^{-3}$	Pas
Gas density	100.0	kg/m^3
Gas viscosity	$1.8\cdot10^{-5}$	Pas
Solids density	$2.0\cdot10^{3}$	kg/m^3
Surface tension	0.073	N/m
Normal restitution coefficient	1.00	
Tangential restitution coefficient	1.00	
Friction coefficient coefficient	0.00	
$-\log(\mathrm{Mo})$	10.6	
Eo	0.48	

Simulation set-up

The simulations are started with a random initial configuration of bubbles and particles, generated using a Monte-Carlo method. In this method, the dispersed elements (bubbles/particles) are first placed in a lattice structure in the domain. Subsequently, each element is displaced slightly 200 times. The procedure is repeated until no overlap between the elements is found.

In the simulations, periodic boundaries are used to mimic an infinite bubble/particle swarm. To ensure that the finite box size does not influence the results, a minimum number of bubbles and particles is required. Roghair *et al.* (2011) and Bunner and Tryggvason (2002) established that the minimum number of bubbles needed is 12. By changing the number of particles for simulations with the settings of table 1, there is no effect when the number of particles exceeds 40. Therefore, the minimum number of bubbles and particles used in the simulations is conservatively set to respectively 16 and 60.

Besides the number of bubbles and particles, the resolution of both the particles and the bubbles should be sufficient to obtain grid independent results. Dijkhuizen *et al.* (2010a) showed that at least 20 grid cells across a bubble diameter are needed in the used FT method. Furthermore, simulations using again the settings of table 1 with a different resolution for the particles showed negligible effect of the grid resolution. Therefore, the number of grid cells inside a particle and a bubble diameter is set to 10 and 20, respectively.

To study the effect of the void fraction and the solids volume fraction, 27 different simulations have been performed, which are grouped in four different cases listed in table 2. All

Table 2: Gas fraction, solids volume fraction and averaging time for the four different cases studied to determine the effect of solids volume fraction and the void fraction. All cases have the same settings as listed in table 1, except for the parameters listed here.

Case	α	ϕ	t_{avg}
1	0.20	0.02...0.14	0.8
2	0.40	0.02...0.14	0.25...0.8
3	0.15...0.45	0.05	0.55...0.8
4	0.15...0.45	0.10	0.8

simulations are initiated with a time step of $1.0 \cdot 10^{-5}$ s and continued for 1 s. To remove any start-up effects, the first 0.2 s is discarded from the analysis, which was sufficient to yield the time-averaged slip velocity within 2% from the final results for two phase flows (Roghair *et al.*, 2011).

RESULTS

First, the effect of the particles on the bubble drag force is quantified by varying the solids volume fraction and the void fraction. The drag coefficient of the bubbles is determined using a macroscopic force balance for the bubbles similar to the work of Roghair *et al.* (2011). At a pseudo steady state, the time-averaged drag will exactly balance the gravitational force and the hydrostatic pressure force in the flow direction.

$$\begin{aligned} < \mathbf{F}_D > &= < \mathbf{F}_G > + < \mathbf{F}_P > \\ &= V_b \rho_g \mathbf{g} - \nabla p V_b \\ \frac{1}{2}\rho_l \mathbf{v}_{rel,b}^2 C_D \frac{\pi d_b^2}{4} &= \left(1 - \alpha - \phi \frac{\rho_l - \rho_s}{\rho_l - \rho_g}\right)(\rho_l - \rho_g) g_z V_b \end{aligned} \quad (7)$$

The relative drag coefficient can be obtained by normalizing the drag coefficient of equation 7 with the drag coefficient of a single bubble rising in an infinite pool of liquid obtained by Tomiyama (1998). This definition results in a direct correspondence between the relative drag coefficient and the terminal rise velocity of a single bubble with the same size and the average velocity of the bubbles in the simulation. Because the addition of particles and the other bubbles results in a difference in hydrostatic pressure in comparison with a single rising bubble, the bubble rise velocity has to be corrected with the void fraction and the solids volume fraction, equation 8. It should be noted that this equation reduces to the form of Roghair *et al.* (2011) in the absence of particles or when the particles are neutrally buoyant.

$$C_{D,rel} = \frac{C_D}{C_{D,\infty}\left(1 - \alpha - \phi \frac{\rho_l - \rho_s}{\rho_l - \rho_g}\right)} = \frac{< \mathbf{v}_{b,\infty} >^2}{(< \mathbf{v}_b > - < \mathbf{u} >)^2} \quad (8)$$

Figure 1 shows the relative drag coefficients resulting from the three-phase simulations including the standard deviations. For case 2, two different simulations with a solids volume fraction of 8% but different initial positions are shown. The figure shows that the relative drag coefficients differ only 12%, which is within the large and overlapping standard deviation. In addition, the standard deviations obtained in this work are larger than those obtained for gas-liquid bubble swarms, which is probably due to the interactions with the (heavier) particles.

According to figure 1, the drag coefficient of the bubbles increases with increasing void fraction and solids volume fraction. The increase of the relative drag force with increasing void fraction was also determined in two-phase flows (Roghair *et al.*, 2011; Martínez-Mercado *et al.*, 2007). However, the effects in the three-phase flow are larger due to the addition of particles, which is in good agreement with the experimentally observed decrease in the bubble rise velocity upon the introduction of particles (Kantarci *et al.*, 2005; Wang *et al.*, 2007; Hooshyar *et al.*, 2013; Pan *et al.*, 2016).
The data of figure 1 was used to derive a correlation for the relative bubble drag coefficient. With respect to the form of the correlation, we constrained the form such that the correlation will lead to the correlation of Roghair *et al.* (2011) in the limit that there are no particles ($\phi = 0$) and that the drag coefficient of a single bubble ($\alpha = 0$) is higher in a liquid containing particles. This resulted in the fit in equation 9.

$$C_{D,rel} = 1 + \frac{18}{\mathrm{Eo}}\alpha + 1.8 \cdot 10^5 \alpha^5 \phi^{1.1} + 2.7 \cdot 10^3 \phi^2 \quad (9)$$

In addition to the close match of the symbols and the lines in figure 1, the parity plot of figure 2 shows that most of the results are within 10% of the fit. On average, the differences between the correlation and the simulation results amounts 7.6%, which is less than the spread in results obtained by using different initial conditions. The maximum difference, which is obtained for low solids volume fractions and low void fractions, is 20%.
Secondly the effect of the bubbles on the drag coefficient of the particles can be determined in a similar manner as the drag coefficient of the bubbles. In the case of the particles, the drag coefficient is now normalized with the drag coefficient of a single particle in an infinite fluid, given by Schiller and Nauman (Clift *et al.*, 1978):

$$C_{D,\infty,p} = \frac{4 d_p (\rho_l - \rho_p) g_z}{3 \rho_l w_z^2} = \frac{24}{\mathrm{Re}_p}\left(1 + 0.15 \mathrm{Re}_p^{0.687}\right) \quad (10)$$

The resulting relative drag coefficient is given by:

$$C_{D,rel,p} = \frac{C_D}{C_{D,\infty,p}\left(1 - \phi - \alpha \frac{\rho_g - \rho_l}{\rho_s - \rho_l}\right)} = \frac{< \mathbf{w}_\infty >^2}{(< \mathbf{w}_p > - < \mathbf{u} >)^2} \quad (11)$$

Figure 3 clearly shows that the drag force on the particles occasionally changes direction. In these circumstances, a bubble and particle will mutually rise, because the combination of one bubble and one particle is buoyant with respect to the liquid. The large standard deviations indicate that particles have two different modes: almost free movement and movement that is obstructed by bubbles. Because particles appear to alternate between these modes, the standard deviations are much larger than the averaged drag coefficient. The calculation of the drag coefficient will be improved when the drag coefficient is calculated for each of these two modes separately. However, this is beyond the scope of this work. In addition, the simulations of case 2 with a solids fraction of 8% only show a difference of 8% for the drag coefficient of the particles.
The obtained drag coefficients are also fitted to quantify the effect of the void fraction and the solids volume fraction on the drag coefficient. The correlation should meet two criteria: the relative drag coefficient of the particles should be equal to 1 when the solids volume fraction and the void fraction are zero. Secondly, it is expected that the drag coefficient of a

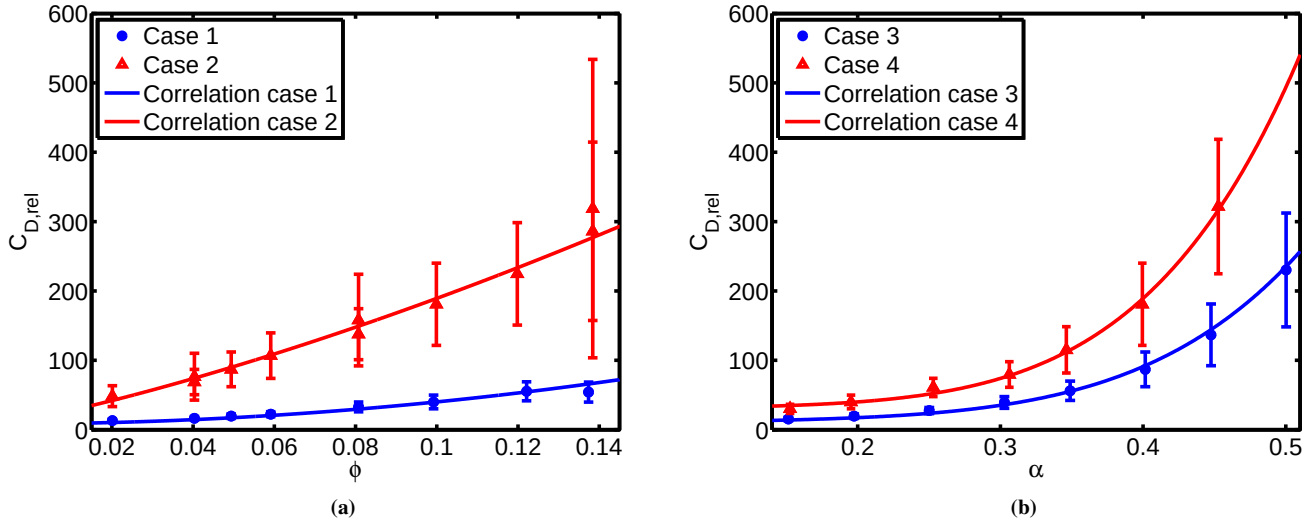

Figure 1: Effect of the solids volume fraction, figure a, and the effect of the void fraction, figure b, on the normalized drag coefficient of the bubbles. The drag is normalized using equation 8. The lines in the figures represent the fit of equation 9. The bars indicate the standard deviation.

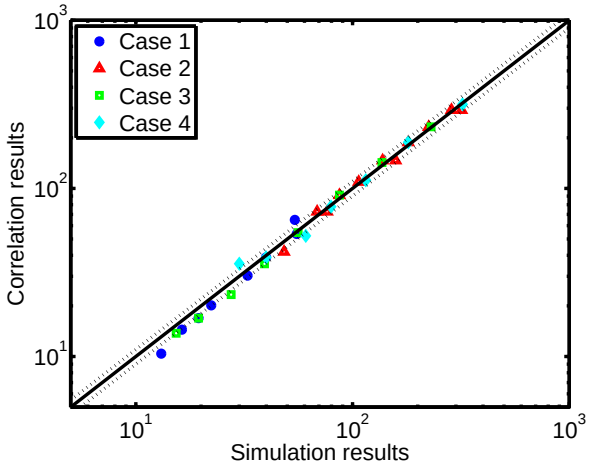

Figure 2: Parity plot containing the relative drag coefficient of the particles obtained from the simulations and the correlation given by equation 9. The dashed lines indicate an error of 10%.

single particle in a bubble swarm or in a particle swarm have a relatively higher drag than a single particle in an infinite liquid. The obtained fit is shown in equation 12.

$$C_{D,rel,p} = 1 + 10\alpha^{2.5} + 200\phi^2 + 1.41 \cdot 10^7 \phi^{4.5}\alpha^5 \qquad (12)$$

In addition to a proper capture of the trends in the drag coefficient, the parity plot in figure 4 shows an average absolute difference between the simulation and the correlation results of only 7.1% with a maximum of 22.5%.

The increase of the drag coefficients of both the bubbles and the particles can partly be explained by the micro structuring of the bubbles. The bubbles cluster in a dynamic system of horizontal layers, as shown in figure 5. The horizontal clustering was already observed by Roghair *et al.* (2013b) for bubble swarms and by Baltussen *et al.* (2013) for slurries, and is probably caused by the lack of large scale circulations. The clustering of the particles prevails due to hindrance by the bubbles. The particles partly cluster on top of the bubbles, effectively hindering the rise of the bubbles, which decreases the particle velocity or even reverses its direction. The particles will eventually roll down the side of the bubble, due to a combination of buoyancy forces and surface tension.

CONCLUSION

In this paper, a combined FT second order implicit IB method was used to simulate dense bubble/particle swarms. By using this method, the effect of the void fraction and the solids volume fraction on the drag coefficient of 1 mm particles and 2 mm bubbles was determined. For both the particles and bubbles, a combined effect of the void fraction and the solids volume fraction was found on the drag coefficient. Using the simulation results, drag correlations for both the bubbles and the particles were developed, which provides an accurate description for $15\% \leq \alpha \leq 50\%$ and $2\% \leq \phi \leq 14\%$.

Because of the limited range in physical properties, particle and bubble diameter used in this paper, the applicability of the obtained correlations is limited to the range of conditions investigated. To obtain a broader applicability, the simulation

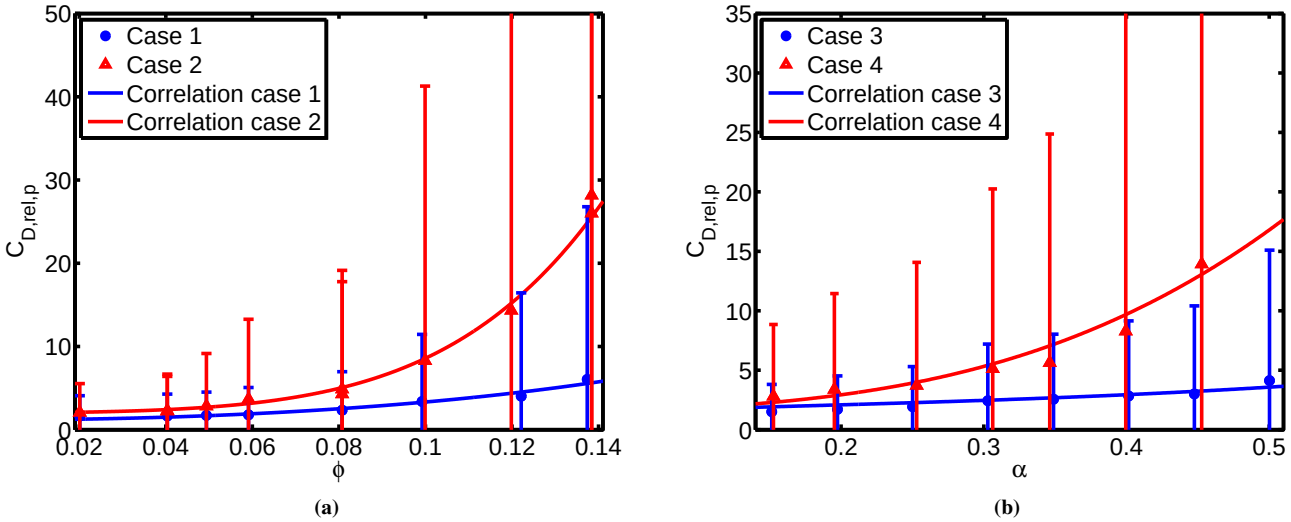

Figure 3: Effect of the solids volume fraction (a), and the effect of the void fraction (b) on the normalized drag coefficient of the particles. The drag is normalized using equation 11. The lines in the figures represent the fit of equation 12. The bars indicate the standard deviation.

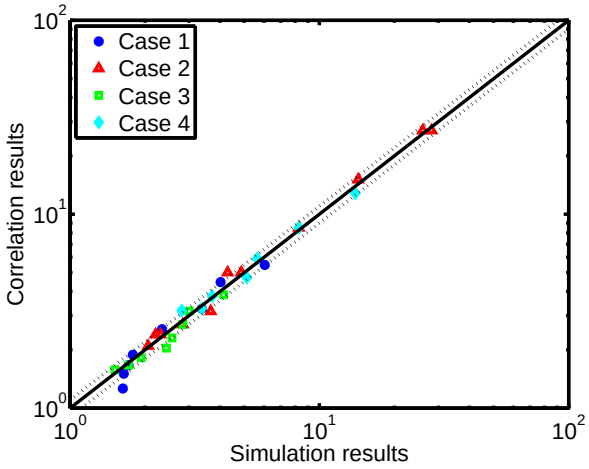

Figure 4: Parity plot containing the relative drag coefficient of the particles obtained from the simulations and the correlation given by equation 12. The dashed lines indicate an error of 10%.

range should be extended. Preliminary results to assess the effect of the bubble diameter show similar trends in void fraction and solids volume fraction. An increasing bubble diameter will lead to a decrease in the drag coefficient for both the bubbles and the particles. It is expected that the size of the particles will influence the drag coefficient. However, because the increase of inertia of the particles might lead to larger deformation and even to break-up of the bubbles, it is hard to predict the effect of the particle size on the drag of both particles and bubbles.

Simulating particles with a high inertia in combination with bubbles with a relatively low surface tension is still difficult for the FT-IB model. In such cases, particles can fall through bubbles, leading to the formation of a doughnut shaped bubble or even the break-up of the bubble. To enable capturing these events, a break-up model needs to be included in the method. Another option is to combine the currently used FT model with the Volume of Fluid model, which prevents unphysical merging of the bubbles while break-up is incorporated in the model (Torres and Brackbill, 2000; Walker *et al.*, 2013). Another option is to implement FT without connectivity, like the Local Front Reconstruction Method (Shin and Juric, 2002).

Although the second order IB method is tested thoroughly, the rotation of freely moving particles at high Reynolds numbers is not accurately calculated. However, the disturbance of the bubbles and the frequent collisions with both particles and bubbles are expected to diminish any effect of unphysical rotation. To prevent any unphysical rotation of the particles, the calculation of the rotational velocity should be improved.

Finally, the currently used size ratio between the bubbles and the particles ($d_b/d_p = 2$) is much larger than the ratio which is common in slurry bubble columns ($d_b/d_p \approx 10 - 100$). To obtain a realistic effect of the particles on the drag of the bubbles and vice versa, this diameter ratio should be decreased drastically. Clearly this will put challenges on the allowable number of grid cells, which can probably only be solved by applying adaptive grid refinement.

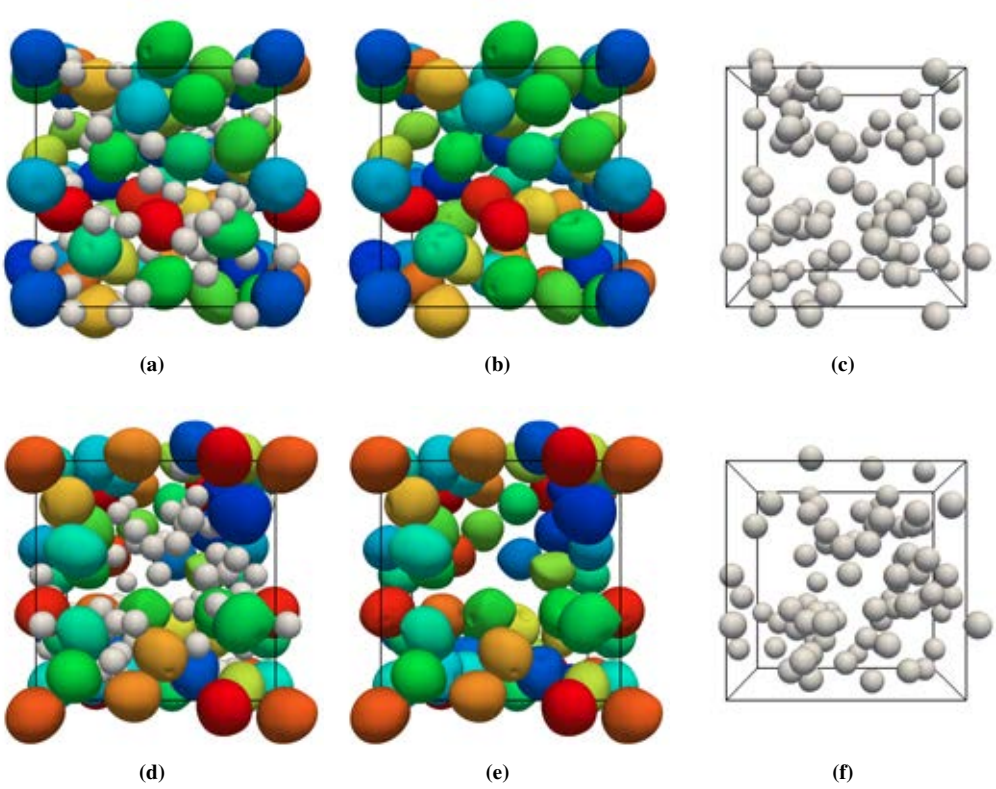

Figure 5: Two snapshots of a simulation with a void fraction of 25% and a solids volume fraction of 5%. Figure (a) and (d) show both the particles and the bubbles, while the middle and the right figures only show the bubble configuration and the particle configuration.

ACKNOWLEDGMENT

The authors would like to thank the European Research Council for its financial support, under its Starting Investigator Grant scheme, contract number 259521 (CuttingBubbles).

REFERENCES

BALTUSSEN, M.W., SEELEN, L.J.H., KUIPERS, J.A.M. and DEEN, N.G. (2013). "Direct numerical simulations of gas-liquid-solid three phase flows". *Chemical Engineering Science*, **100**, 293–299.

BALTUSSEN, M.W., SEGERS, Q.I.E., KUIPERS, J.A.M. and DEEN, N.G. (2016). "Cutting bubbles with a single wire". *Chemical Engineering Science (accepted)*.

BUNNER, B. and TRYGGVASON, G. (2002). "Dynamics of homogeneous bubbly flows part 1. rise velocity and microstructure of the bubbles". *Journal of Fluid Mechanics*, **466**, 17–52.

CLIFT, R., GRACE, J.R. and WEBER, M.E. (1978). *Bubbles, drops and particles*. Academic Press, New York.

DEEN, N.G., van Sint Annaland, M. and KUIPERS, J.A.M. (2004). "Multi-scale modeling of dispersed gas-liquid two-phase flow". *Chemical Engineering Science*, **59(8-9)**, 1853–1861.

DEEN, N.G., van Sint Annaland, M. and KUIPERS, J.A.M. (2009). "Direct Numerical Simulation of complex multi-fluid flows using a combined Front Tracking and Immersed Boundary method". *Chemical Engineering Science*, **64(9)**, 2186–2201.

DEEN, N.G., KRIEBITZSCH, S.H.L., van der Hoef, M.A. and KUIPERS, J.A.M. (2012). "Direct Numerical Simulation of flow and heat transfer in dense fluid-particle systems". *Chemical Engineering Science*, **81**, 329–344.

DIJKHUIZEN, W., ROGHAIR, I., van Sint Annaland, M. and KUIPERS, J.A.M. (2010a). "DNS of gas bubbles behaviour using an improved 3D Front Tracking model–drag force on isolated bubbles and comparison with experiments". *Chemical Engineering Science*, **65(4)**, 1415–1426.

DIJKHUIZEN, W., ROGHAIR, I., van Sint Annaland, M. and KUIPERS, J.A.M. (2010b). "DNS of gas bubbles behaviour using an improved 3D Front Tracking model–model development". *Chemical Engineering Science*, **65(4)**, 1427–1437.

FRANCOIS, M.M., CUMMINS, S.J., DENDY, E.D., KOTHE, D.B., SICILIAN, J.M. and WILLIAMS, M.W. (2006). "A balanced-force algorithm for continuous and sharp interfacial surface tension models within a volume tracking framework". *Journal of Computational Physics*, **213(1)**, 141–173.

GE, Y. and FAN, L.S. (2006). "3-D Direct Numerical Simulation of gas-liquid and gas-liquid-solid flow systems using the Level-Set and Immersed-Boundary methods". *Advances in Chemical Engineering*, **31**, 1–63.

HOOMANS, B.P.B., KUIPERS, J.A.M., BRIELS, W.J. and van Swaaij, W.P.M. (1996). "Discrete Particle simulation of bubble and slug formation in a two-dimensional gas-fluidised bed: A hard-sphere approach". *Chemical Engineering Science*, **51(1)**, 99–118.

HOOSHYAR, N., VAN OMMEN, J.R., HAMERSMA, P.J., SUNDARESAN, S. and MUDDE, R.F. (2013). "Dynamics of single rising bubbles in neutrally buoyant liquid-solid suspensions". *Physical Review Letters*, **110(24)**, 244501.

JAIN, D., DEEN, N.G., KUIPERS, J.A.M., ANTONYUK,

S. and HEINRICH, S. (2012). "Direct Numerical Simulation of particle impact on thin liquid films using a combined Volume of Fluid and Immersed Boundary method". *Chemical Engineering Science*, **69(1)**, 530–540.

KANTARCI, N., BORAK, F. and ULGEN, K.O. (2005). "Bubble column reactors". *Process Biochemistry*, **40(7)**, 2263–2283.

KUPRAT, A., KHAMAYSEH, A., GEORGE, D. and LARKEY, L. (2001). "Volume conserving smoothing for piecewise linear curves, surfaces, and triple lines". *Journal of Computational Physics*, **172**, 99–118.

LI, Y., YANG, G.Q., ZHANG, J.P. and FAN, L.S. (2001). "Numerical studies of bubble formation dynamics in gas-liquid-solid fluidization at high pressures". *Powder Technology*, **116(2-3)**, 246–260.

MARTÍNEZ-MERCADO, J., PALACIOS-MORALES, C. and ZENIT, R. (2007). "Measurement of pseudo-turbulence intensity in monodispersed bubbly liquids for $10<\mathrm{Re}\leq 500$". *Physics of Fluids*, **19(10)**.

PAN, H., CHEN, X.Z., LIANG, X.F., ZHU, L.T. and LUO, Z.H. (2016). "Cfd simulations of gasâĂŞliquidâĂŞsolid flow in fluidized bed reactors - a review". *Powder Technology*, **299**, 235–258.

RAESSI, M., MOSTAGHIMI, J. and BUSSMANN, M. (2010). "A Volume-of-Fluid interfacial flow solver with advected normals". *Computers & Fluids*, **39(8)**, 1401–1410.

RENARDY, Y. and RENARDY, M. (2002). "PROST: A parabolic reconstruction of surface tension for the Volume-of-Fluid method". *Journal of Computational Physics*, **183(2)**, 400–421.

ROGHAIR, I. (2012). *Direct Numerical Simulations of Hydrodynamics and Mass Transfer in Dense Bubbly Flows*. Ph.D. thesis, Eindhoven, University of Technology.

ROGHAIR, I., LAU, Y.M., DEEN, N.G., SLAGTER, H.M., BALTUSSEN, M.W., van Sint Annaland, M. and KUIPERS, J.A.M. (2011). "On the drag force of bubbles in bubble swarms at intermediate and high reynolds numbers". *Chemical Engineering Science*, **66**, 3204–3211.

ROGHAIR, I., BALTUSSEN, M.W., van Sint Annaland, M. and KUIPERS, J.A.M. (2013a). "Direct Numerical Simulations of the drag force of bi-disperse bubble swarms". *Chemical Engineering Science*, **95**, 48–53.

ROGHAIR, I., VAN SINT ANNALAND, M. and KUIPERS, J.A.M. (2013b). "Drag force and clustering in bubble swarms". *AIChE Journal*, **59(5)**, 1791–1800.

SHIN, S. and JURIC, D. (2002). "Modeling three-dimensional multiphase flow using a level contour reconstruction method for Front Tracking without connectivity". *Journal of Computational Physics*, **180**, 427–470.

TOMIYAMA, A. (1998). "Struggle with computational bubble dynamics". *Third International Conference on Multiphase Flow*, 369–405.

TORRES, D.J. and BRACKBILL, J.U. (2000). "The Point-Set method: Front-Tracking without connectivity". *Journal of Computational Physics*, **165(2)**, 620–644.

van Sint Annaland, M., DEEN, N.G. and KUIPERS, J.A.M. (2003). *Multi-level modeling of dispersed gas-liquid two-phase flows*. Heat and mass transfer. Springer, Berlin (edited by M. Sommerfeld and D. Mewes).

WALKER, E., NIKITOPOULOS, D. and TROMEUR-DERVOUT, D. (2013). "Parallel solution methods for poisson-like equations in two-phase flows". *Computers & Fluid*, **80**, 152–157.

WANG, T., WANG, J. and JIN, Y. (2007). "Slurry reactors for gas-to-liquid processes: A review". *Industrial and Engineering Chemistry Research*, **46(18)**, 5824–5847.

YANG, G.Q., DU, B. and FAN, L.S. (2007). "Bubble formation and dynamics in gas-liquid-solid fluidization. a review". *Chemical Engineering Science*, **62(1-2)**, 2–27.

ZICK, A.A. and HOMSY, G.M. (1982). "Stokes flow through periodic arrays of spheres." *Journal of Fluid Mechanics*, **115**, 13–26.